N93-15508

Instrumentation of the variable-angle magneto-optic ellipsometer and its application to m-o media and other non-magnetic films

Andy F. Zhou, J. Kevin Erwin and M. Mansuripur

Optical Sciences Center, University of Arizona, Tucson, AZ 85721

ABSTRACT

A new and comprehensive dielectric tensor characterization instrument is presented for characterization of magneto-optical recording media and non-magnetic thin films. Random and systematic errors of the system are studied. A series of TbFe, TbFeCo, and Co/Pt samples with different composition and thicknesses are characterized for their optical and magneto-optical properties. The optical properties of several non-magnetic films are also measured.

I. INTRODUCTION

Dielectric tensor ε characterization of M-O recording media is important for their application. It gives the important parameters like the reflectivity of the material, and, more importantly, the magneto-optic Kerr effect is determined from it. The traditional method of measuring ε consists of two steps. First using an ellipsometer[1] one obtains the refractive index n and absorption coefficient k, which are directly related to the diagonal element of the dielectric tensor. The second step consists of measuring the Kerr rotation angle θ_k and ellipticity ϵ_k using one of several available techniques[1-7] at normal incidence. From these measurements and the knowledge of n and k, the off-diagonal element of the dielectric tensor is calculated.[8] Connell used this method to obtain the dielectric tensor for a set of rare earth-transition metal alloy thin films.[9] Recently there have been some reported measurements for Co/Pt and Co/Pd superlattice samples.[10, 11] This traditional method usually requires that the magneto-optical film is thick enough to be opaque (thicker than 400 Å for TbFe and superlattice samples). This limits the application of this method and is not suitable for very thin samples which are important for application, especially the superlattice samples.

In this paper we use a new and comprehensive method[12, 13] to characterize the dielectric tensor of magneto-optical thin film samples. This method applies for all thicknesses and the measurements are done with a single apparatus. With a multilayer analysis program[14], the dielectric tensor as well as the film thickness for each layer of a multilayered film can be determined. The apparatus is also useful for determining the refractive index n, absorption coefficient k and film thickness of various layers of a multilayered non-magnetic film.

The paper is arranged as follows. In Sec. II, We discuss the principles of the technique. The experimental set up, calibration and performance analysis are discussed in detail. In Sec. III, we present some measurement results of TbFe and Co/Pt samples with various thicknesses and compositions. Various non-magnetic samples of glass, dielectric, sol-gel, organic polymer, and metals are studied in Sec. IV. Section V is the summary.

II. SYSTEM SETUP AND ANALYSIS

We first define the physical content of the dielectric tensor measured by this system. With the magnetization along the z-axis (perpendicular to the x-y plane of the film), the dielectric tensor ε is written as:[15]

ORIGINAL PAGE IS
OF POOR QUALITY

PRECEDING PAGE BLANK NOT FILMED

$$\varepsilon = \begin{bmatrix} \varepsilon_{xx} & \varepsilon_{xy} & 0 \\ -\varepsilon_{xy} & \varepsilon_{yy} & 0 \\ 0 & 0 & \varepsilon_{zz} \end{bmatrix} . \tag{1}$$

Since the film is believed to be structurally isotropic, we shall assume $\varepsilon_{xx} = \varepsilon_{yy} = \varepsilon_{zz}$. In general, the elements of the tensor are complex. Thus ε_{xx} (the diagonal element), describes the optical properties of the film in the absence of the magneto-optical effects according to the following relation

$$\sqrt{\varepsilon_{xx}} = n + ik \ . \tag{2}$$

The off-diagonal element ε_{xy} is responsible for the magneto-optical Kerr and Faraday effects. Assuming that the Kerr rotation angle θ_k and ellipticity ϵ_k are small, and light is at normal incidence on thick film with no overcoating, the relation between θ_k, ϵ_k, ε_{xx}, and ε_{xy} can be written as

$$\theta_k - i\epsilon_k = \frac{\varepsilon_{xy}}{\sqrt{\varepsilon_{xx}}\,(\varepsilon_{xx} - 1)} \ . \tag{3}$$

This relationship indicates that the magneto-optical Kerr effect is proportional to the off-diagonal element ε_{xy}.

Measurement of the dielectric tensor consists of measuring the complex reflection coefficients of the sample and fitting the parameters into the multilayer analysis program.

II.1. Experimental Setup

Figure 1 shows the experimental setup,[12] called variable-angle magneto-optic ellipsometer (VAMOE). The incident angle A varies from 30° to 88°. The HeNe laser beam ($\lambda = 632.8$ nm) passes through a polarizer and a quarter-wave plate whose fast axis is at 45° to the transmission axis of the polarizer. The polarizer helps to clean the laser beam to be linearly-polarized, and the quarter-wave plate makes the light to become circularly polarized at output. The polarizing beam splitter (PBS) divides the beam into two parts, sending one onto the monitor detector for laser power calibration. The other half passes through the PBS and is focused onto the sample. The PBS sits on a rotating mount and can polarize the incident beam at angle β with the plane of reference. Of those angles, the directions of p (parallel), s (perpendicular), and 45° are the ones used. The circularized light before the PBS keeps the light power incident on the sample constant for any β angle, which lets us use a constant gain for detecting circuitry. The electro-magnet behind the sample applies a magnetic field with the strength of ±7.5 kOe.

After reflecting from the sample, the beam passes through another quarter-wave plate, whose fast axis is at $\zeta = 45°$ to the reference plane. The beam then goes through a Wollaston prism and is finally detected by two detectors. The Wollaston prism and the photodetectors sit on a rotation stage whose axis is aligned with the beam. This rotation stage allows the axis of the Wollaston to be set at angle η relative to the reference plane; $\eta = 0°$ and 45° are used in this experiment. The two photodetectors are identical, and their conversion factor, defined as the ratio of the output voltage to the input light intensity is α. We will denote the individual detector output by S_1 and S_2, their sum by σ, and their difference, which appears at the output of the differential amplifier, by ΔS.

To normalize the measurement results we must know the effective light amplitude that goes through the system. This can be measured by removing the sample and setting the incident angle A = 90°. If the effective light amplitude is denoted C, the sum of the signals S_1 and S_2 will be given by

$$\sigma_0 = \frac{1}{2}\alpha C^2 \quad . \tag{4}$$

In the following discussion we will assume that the results are normalized by σ_0.

As for the discussion of the measurement technique, let us define the notation. The linearly polarized incident light with polarization direction in the plane of incidence (also the plane of reference) is the p light, while the light polarized perpendicular to this plane is the s light. For p incident light, the ordinary reflected amplitude and phase are defined as r_p and ϕ_p, respectively. Similarly for s incident light, the ordinary reflected amplitude and phase are r_s and ϕ_s. For magneto-optical samples the p (or s) incident light not only causes ordinary reflection in p (or s) direction but also induces a magneto-optical component in the s (or p) direction. We denote the amplitude and phase of this magneto-optical reflection coefficient by $r_\perp$ and $\phi_\perp$, respectively.

When the sample is placed in the system, the signals S_1 and S_2 will in general depend on r_p, ϕ_p, r_s, ϕ_s, $r_\perp$ and $\phi_\perp$, as well as on β, ζ and η. Then, the sum and difference signals between S_1 and S_2 are derived[12]

$$\begin{aligned}\sigma/\sigma_0 = {} & r_p^2\cos^2\beta + r_s^2\sin^2\beta + r_\perp^2 \\ & + [r_p r_\perp\cos(\phi_p-\phi_\perp) - r_s r_\perp\cos(\phi_s-\phi_\perp)]\sin 2\beta \quad ,\end{aligned} \tag{5}$$

and

$$\begin{aligned}\Delta S/\sigma_0 = {} & [(r_p^2\cos^2\beta - r_s^2\sin^2\beta)\cos 2\zeta \\ & - r_\perp^2\cos(2\beta-2\zeta)]\cos(2\eta-2\zeta) \\ & + r_p r_s[\sin 2\zeta\cos(\phi_p-\phi_s)\cos(2\eta-2\zeta) \\ & + \sin(\phi_p-\phi_s)\sin(2\eta-2\zeta)]\sin 2\beta \\ & - 2r_p r_\perp[\cos\beta\sin(\phi_p-\phi_\perp)\sin(2\eta-2\zeta) \\ & + \sin(2\zeta-\beta)\cos(\phi_p-\phi_\perp)\cos(2\eta-2\zeta)]\cos\beta \\ & - 2r_s r_\perp[\sin\beta\sin(\phi_s-\phi_\perp)\sin(2\eta-2\zeta) \\ & - \cos(2\zeta-\beta)\cos(\phi_s-\phi_\perp)\cos(2\eta-2\zeta)]\sin\beta\end{aligned} \quad . \tag{6}$$

Seven different experimental set-ups are used to fully characterize the sample. They are combinations of different angles of β and η, while keeping $\zeta = 45°$. The seven curves with the setting specifications are listed at Table I.

For measuring the dielectric tensor, these seven different combinations of reflection coefficients versus the incident angle A are measured. Of these, three curves are optical reflectivities, which are independent of magnetic states of the samples, and are obtained with the magnet turned off, while the other four curves are measured with the sample saturated by the magnetic field and are called magneto-optic reflectivity curves. For non-magnetic materials, all the M-O reflection coefficients are zero and only the first three curves are measured.

After measuring these seven curves, a multilayer analysis program[14] is used to analyze the data and estimate the dielectric tensor of the film. This analysis program can deal with multilayer structures containing an arbitrary number of dielectric, metal and magnetic layers. An algorithm based on 2 × 2 matrices is used for the reflection calculation. In this calculation, the incident beam is assumed to be plane monochromatic with arbitrary angle of incidence. There are no approximations involved and the results are direct consequences of Maxwell's equations.

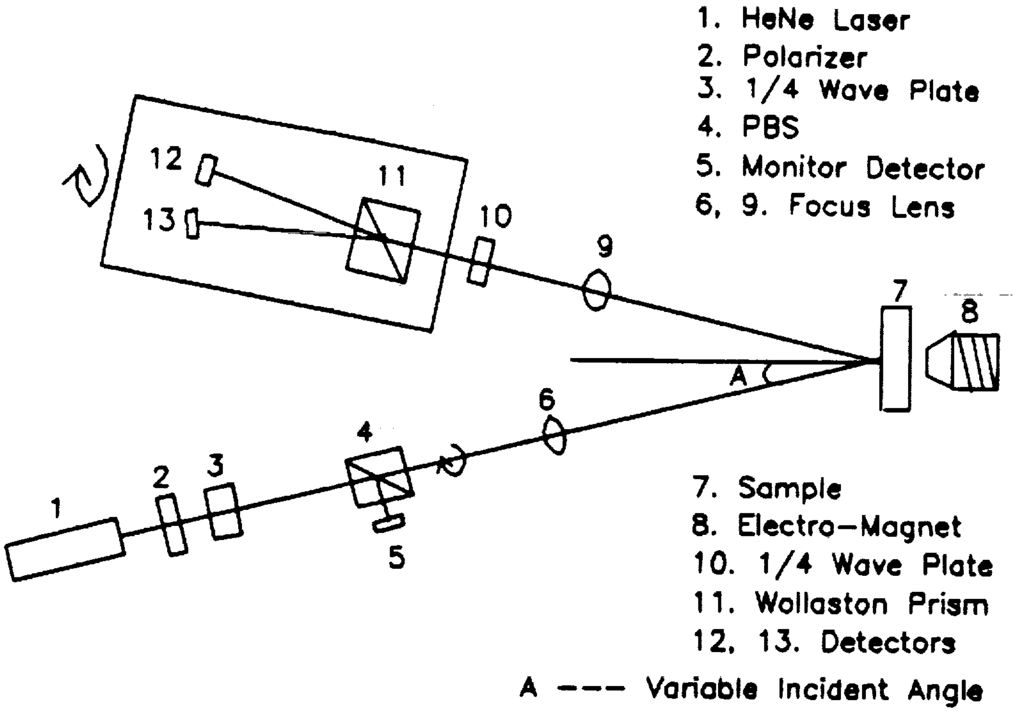

Figure 1. System setup for the variable-angle magneto-optic ellipsometer.

Table I. The measured reflectivity curves. $\zeta = 45°$ for all the measurements.

Curve #	Detector Signal Used	PBS Setting $\beta(°)$	Wollaston Setting $\eta(°)$	Physical description
1	σ/σ_0	0	45	r_p^2
2	σ/σ_0	90	45	r_s^2
3	$\Delta S/\sigma_0$	45	45	$r_p r_s \cos(\phi_p - \phi_s)$
4	$\Delta S/\sigma_0$	0	45	$r_p r_\perp \cos(\phi_p - \phi_\perp)$
5	$\Delta S/\sigma_0$	0	0	$r_p r_\perp \sin(\phi_p - \phi_\perp)$
6	$\Delta S/\sigma_0$	90	45	$r_s r_\perp \cos(\phi_s - \phi_\perp)$
7	$\Delta S/\sigma_0$	90	0	$r_s r_\perp \sin(\phi_s - \phi_\perp)$

II.2. Error Analysis

There are basically two types of error, random and systematic, in this dielectric tensor characterization system. Random errors come from the vibration of the system, fluctuations of the laser power, the random noise in the circuitry and the numerical errors of the multilayer analysis program. Since the individual analysis of them is complicated, we choose to experimentally measure their combined effect.

The random error in the VAMOE system is expressed in the random fluctuation of the measured data. The effect of this error could be different for different types of samples, due to their different shapes of reflectivity curves. To a good estimation, we measured three typical samples. A piece of glass (microscope-slide) which has only n value (k is so close to zero, that its measurement is below the resolution of this system) is typical for dielectric materials. A Co/Pd multilayered thin film with thickness of 165 Å is used as a typical sample for the superlattice materials. A TbFe sample (with overcoating) is typical for the RE-TM materials.

Figure 2 shows the measured reflectivity curves for four independent measurements of the glass sample. The back of the microscope-slide was ground and blackened by ink, in order to reduce reflection from the back surface. As can be seen in Fig. 2, the four independent measurements are coincide with each other. Table II lists the matched n values for each measurement. The data matching error (DME) in this and later tables is the average percent deviation for each data point between the measured data and the calculated data from the multilayer analysis program by using matched parameter(s). The matching error is less than 3% and the standard deviation of the four results is 0.5%.

Figure 3 is the corresponding three independent measurements for a Co(2Å)/Pd(9Å) sample. This sample is sputtered on glass at 7 mtorr of Kr gas, and the total thickness is 165 Å. There is no overcoating. The M-O reflectivity curves have larger difference among the three independent measurements than the curves 1 to 3, which is due to the much smaller signal for these M-O data. Table III is the corresponding results for the Co/Pd sample. The results in the parenthesis (also in the later tables) are measured by our variable wavelength Kerr rotation angle and ellipticity measuring system called magneto-optic Kerr spectrometer (MOKS).[5,6] MOKS measures the Kerr rotation angle and ellipticity using a different method from that of the VAMOE system.

The three measurements of the seven reflection curves for a $Tb_{22.1}Fe_{77.9}$ sample are shown in Fig. 4. The M-O film thickness is 1354 Å. The overcoating is $Si_{32.1}O_{67.9}$ and the estimated thickness is 1264 Å. The thickness measured by this system (the t_{SiO} in the table) is 1326 Å. For the SiO overcoating we use $n = 1.449$ and $k = 0$ for the calculation. Table IV lists the computed parameters for the TbFe sample. Connell's measurement for a $Tb_{21}Fe_{79}$ sample[9] is cited here for comparison.

From the measurements for the three typical samples, we can see that the data matching error is less than 5% and the random error is within the range of tolerance. The slightly larger DME for the TbFe sample is due to its higher complexity with overcoating. The random errors for the Kerr rotation angle, ellipticity and reflectivity are much smaller, which indicates their less sensitivity to fluctuation. The smaller random error for the off-diagonal element of the TbFe sample is due to its much larger magneto-optical reflectivity.

There are at least five possible systematic error sources in the system. One is the incident angle error. We measured this angle by the top view pictures, taken by a camera, for angles from 26° to 90° (with one degree increment). After this, the error on the angle measurements, or the error on the mechanical movements on the rail will be random and they fall into the category of the random error analysis discussed above. The second error source is the gains in the two signal channels and the differential channel of the amplifier circuit. The circuit has been stabilized and calibration was done to wipe out any sizable systematic error on this part. The other three error sources are the accuracy of the polarizer angle for the incident beam, the accuracy of the quarterwave plate angle and the accuracy on the angle readings of the detector box.

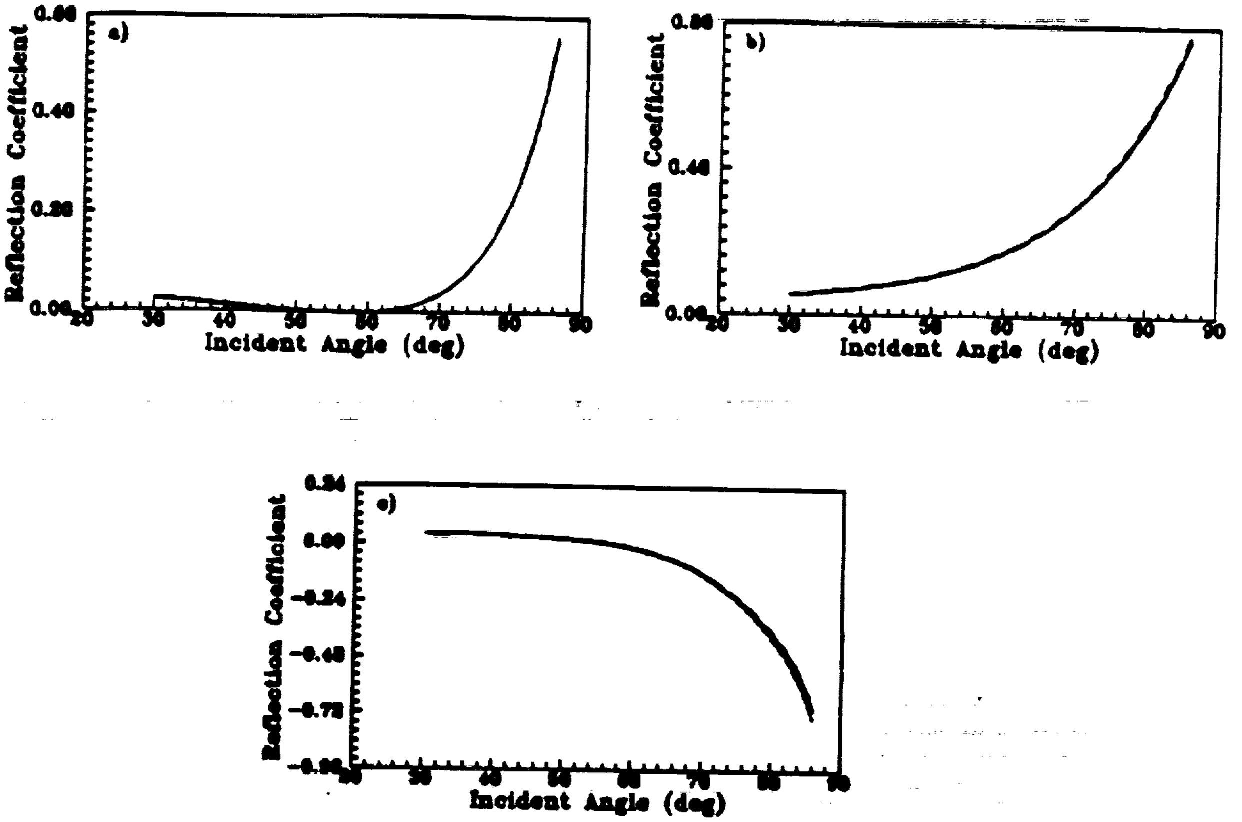

Figure 2. The four independently measured reflection curves (measurements 1 - 4 are "————", "- - - -", "— — —" and "—— ——" lines, respectively) of (a) curve 1, (b) curve 2 and (c) curve 3 for a glass sample.

Table II. Matched values of n for the four measurements of glass.

#	1	2	3	4	average	σ_{n-1}
n	1.496	1.499	1.498	1.512	1.501	0.007
DME (%)	1.9	2.8	2.9	1.1	—	—

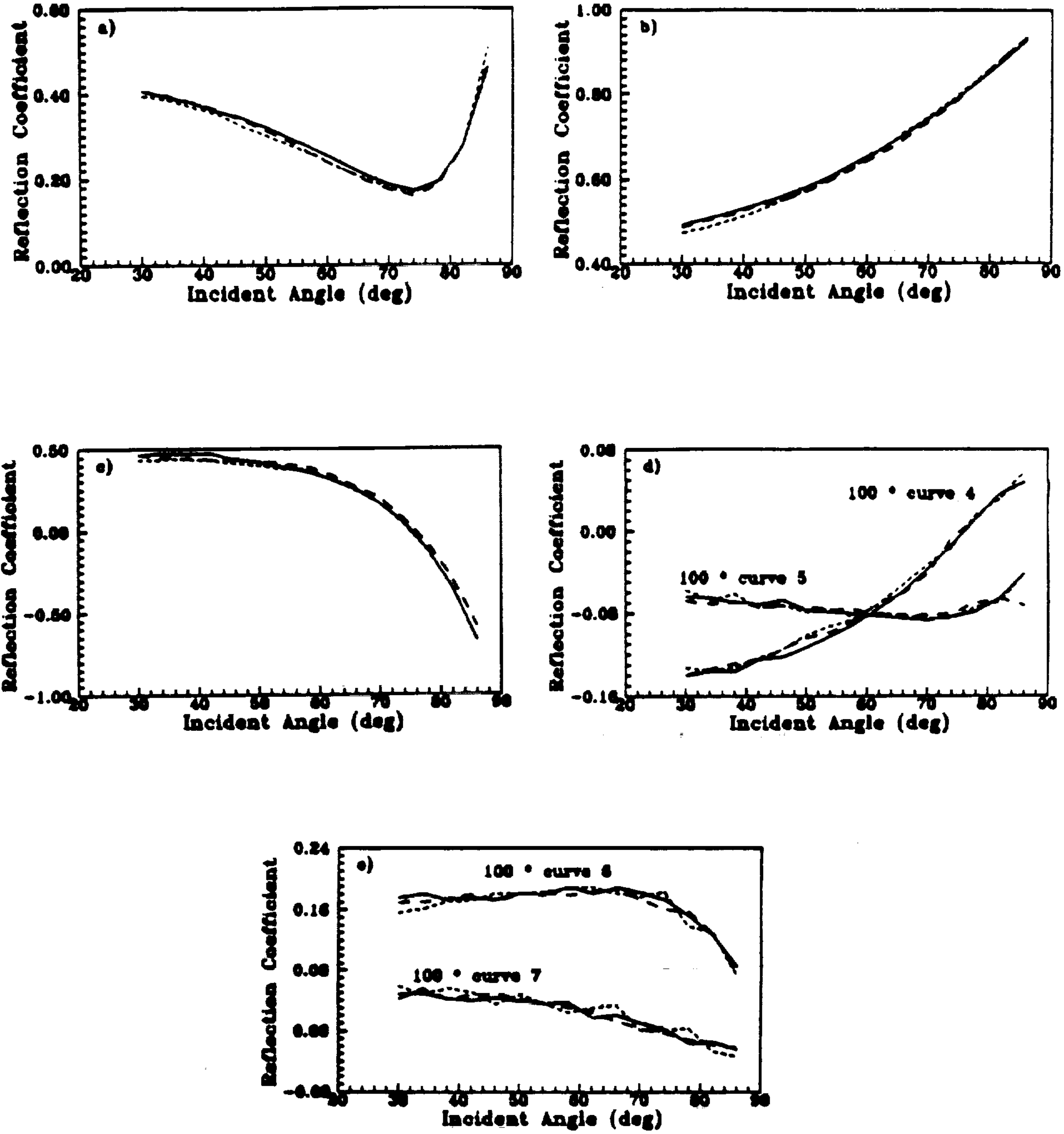

Figure 3. The three independently measured reflection curves (measurements 1 - 3 are "————", "- - - -" and "— — —" lines, respectively) of (a) curve 1, (b) curve 2, (c) curve 3, (d) curves 4 and 5, and (e) curves 6 and 7 for a Co/Pd sample.

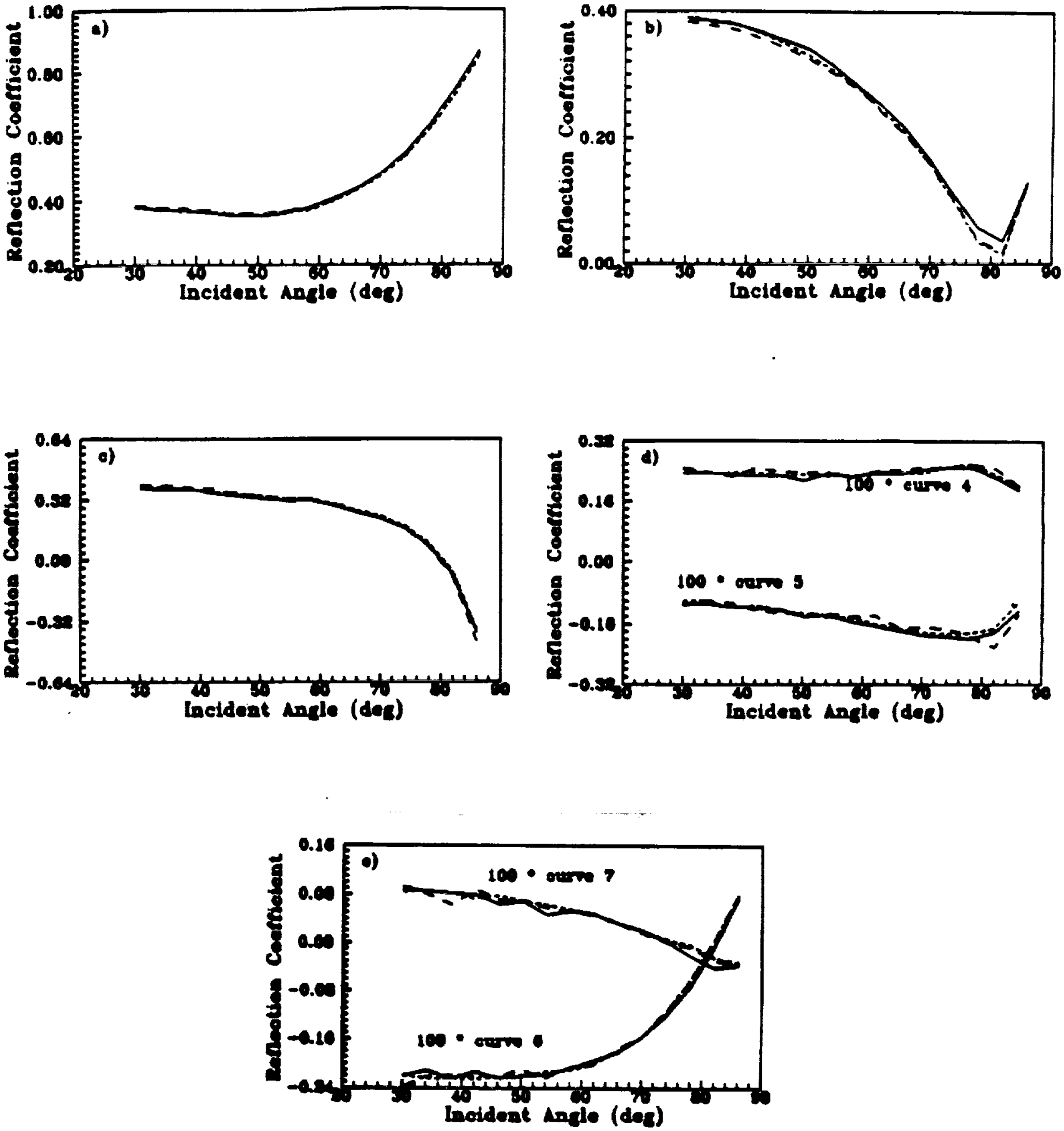

Figure 4. The three independently measured reflection curves (measurements 1 - 3 are "————", "- - - -" and "— — —" lines, respectively) of (a) curve 1, (b) curve 2, (c) curve 3, (d) curves 4 and 5, and (e) curves 6 and 7 for a TbFe sample.

Table III. Three measurements for the Co/Pd sample. The results in the parenthesis are measured from the MOKS system.

#	1	2	3	average	σ_{n-1}
n	1.46	1.42	1.75	1.54	0.2
k	3.81	3.71	3.84	3.79	0.07
ε_{xx}	-12.4 + i11.1	-11.8 + i10.5	-12.0 + i12.6	-12.1 + i11.4	0.3 + i1.0
ε_{xy}	0.148 — i0.100	0.138 — i0.100	0.148 — i0.122	0.145 — i0.107	0.006 — i0.013
DME (%)	2.8	3.0	3.0	—	—
θ_k	0.202	0.205	0.201	0.203 (0.19)	0.002
ϵ_k	0.074	0.080	0.073	0.075 (0.06)	0.004
R	0.450	0.436	0.451	0.446 (0.46)	0.008

Table IV. Three measurements for the TbFe sample. The results in the parenthesis are measured from the MOKS system.

#	1	2	3	average	σ_{n-1}	Connell's
n	2.32	2.38	2.40	2.37	0.04	—
k	3.08	3.10	3.14	3.11	0.03	—
t_{SiO}(Å)	1332	1323	1322	1326	6	—
ε_{xx}	-3.94 + i15.5	-3.82 + i15.9	-3.99 + i15.5	-3.92 + i15.6	0.09 + i0.2	-2.87 + i19.9
ε_{xy}	-0.250 — i0.069	-0.254 — i0.065	-0.247 — i0.065	-0.250 — i0.066	0.004 — i0.002	-0.338 — i0.028
DME (%)	3.0	3.0	4.9	—	—	—
θ_k	-0.310	-0.311	-0.312	-0.311 (-0.31)	0.001	-0.305
ϵ_k	0.131	0.131	0.125	0.129 (0.12)	0.003	0.127
R	0.422	0.417	0.418	0.419 (0.42)	0.003	0.420

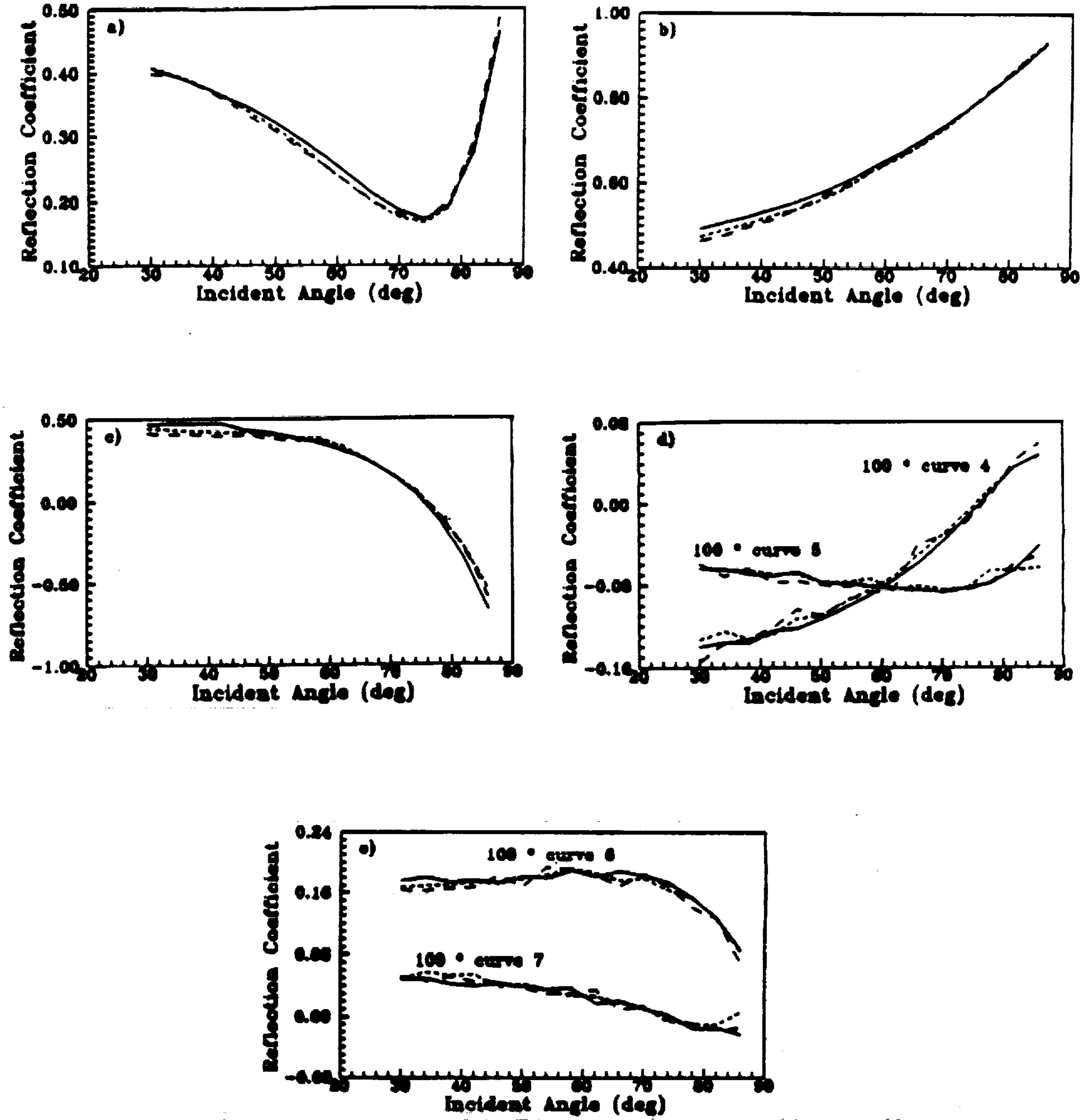

Figure 5. Reflection coefficient measurements for the case that the polarizer angles are at the calibrated angle ("————" line), 2° off ("- - - -" line) and -2° off ("— — —" line), respectively, for systematic error analysis.

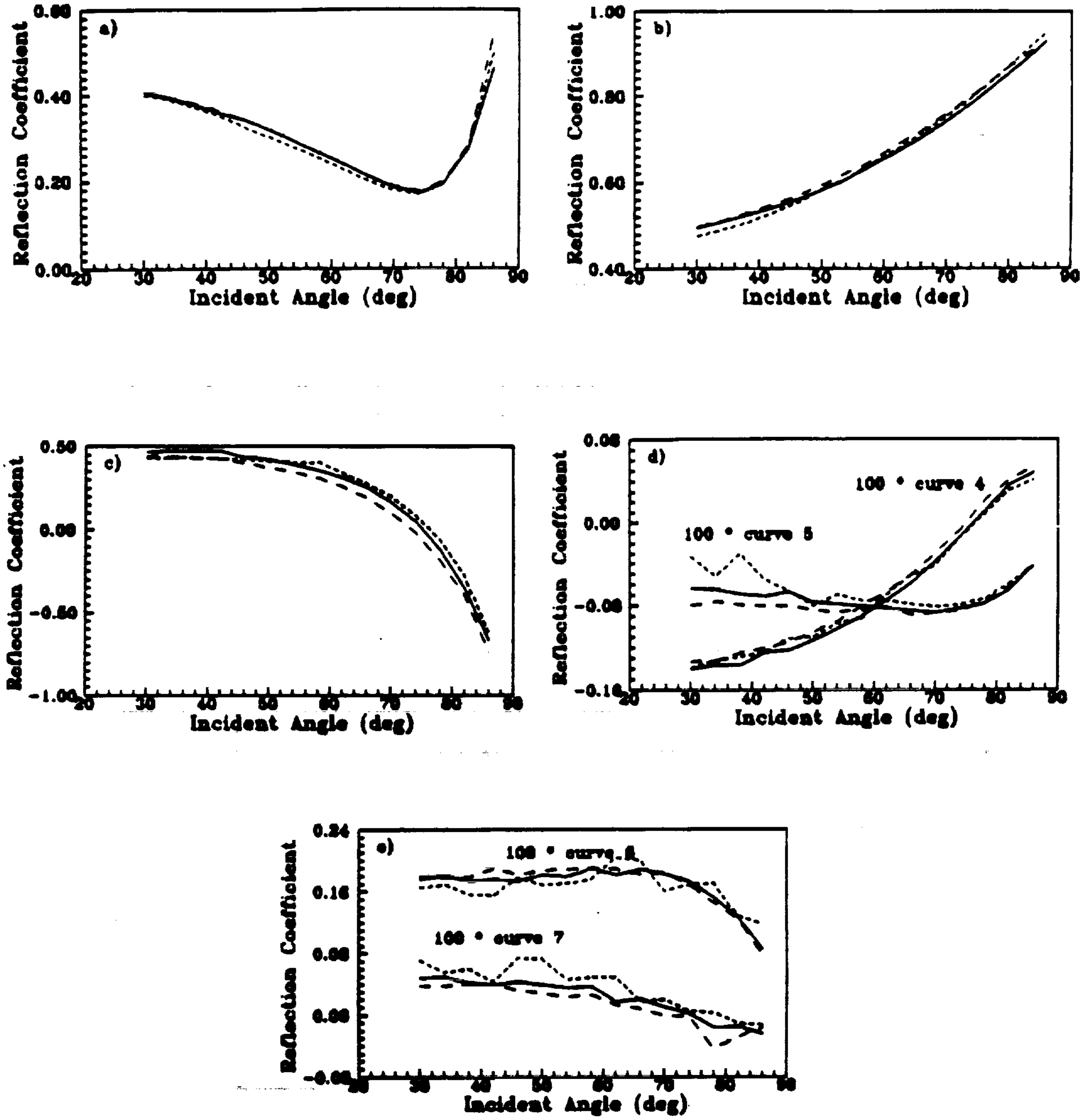

Figure 6. Reflection coefficient measurements for the case that the quarterwave plate are at the calibrated angle ("————" line), 2° off ("- - - -" line) and -2° off ("— — —" line), respectively, for systematic error analysis.

Table V. Measurements for the case that the polarizer angle is ±2° off the calibrated angle for the Co/Pd sample.

	average (no shift)	σ_{n-1} (no shift)	polarizer off 2°	Δ (off 2°)	polarizer off -2°	Δ (off -2°)
n	1.54	0.2	1.67	0.13	1.53	-0.01
k	3.79	0.07	3.78	-0.01	3.72	-0.07
ε_{xx}	-12.1 + i11.4	0.3 + i1.0	-11.4 + i12.4	-0.7 + i1.0	-11.7 + i10.6	0.4 + -i0.8
ε_{xy}	0.145 — i0.107	0.006 — i0.013	0.140 — i0.124	-0.005 — i0.017	0.137 — i0.101	-0.008 — i0.006
DME (%)	3.0	—	3.1	—	3.9	—
θ_k	0.203	0.002	0.203	0	0.205	0.002
ϵ_k	0.075	0.004	0.075	0	0.080	0.005
R	0.446	0.008	0.441	-0.005	0.436	-0.010

Table VI. Measurements for the case that the quarterwave plate angle is ±2° off the calibrated angle for the Co/Pd sample.

	average (no shift)	σ_{n-1} (no shift)	1/4 λ off 2°	Δ (off 2°)	1/4 λ off -2°	Δ (off -2°)
n	1.54	0.2	1.58	0.04	0.92	-0.62
k	3.79	0.07	3.78	-0.01	3.67	-0.12
ε_{xx}	-12.1 + i11.4	0.3 + i1.0	-11.5 + i12.7	0.06 + i1.3	-12.43 + i6.77	-0.3 + -i4.6
ε_{xy}	0.145 — i0.107	0.006 — i0.013	0.135 — i0.132	-0.01 — i0.025	0.130 — i0.047	-0.015 — -i0.060
DME (%)	3.0	—	5.5	—	4.0	—
θ_k	0.203	0.002	0.196	-0.007	0.208	0.005
ϵ_k	0.075	0.004	0.082	0.007	0.078	0.003
R	0.446	0.008	0.444	-0.002	0.441	-0.005

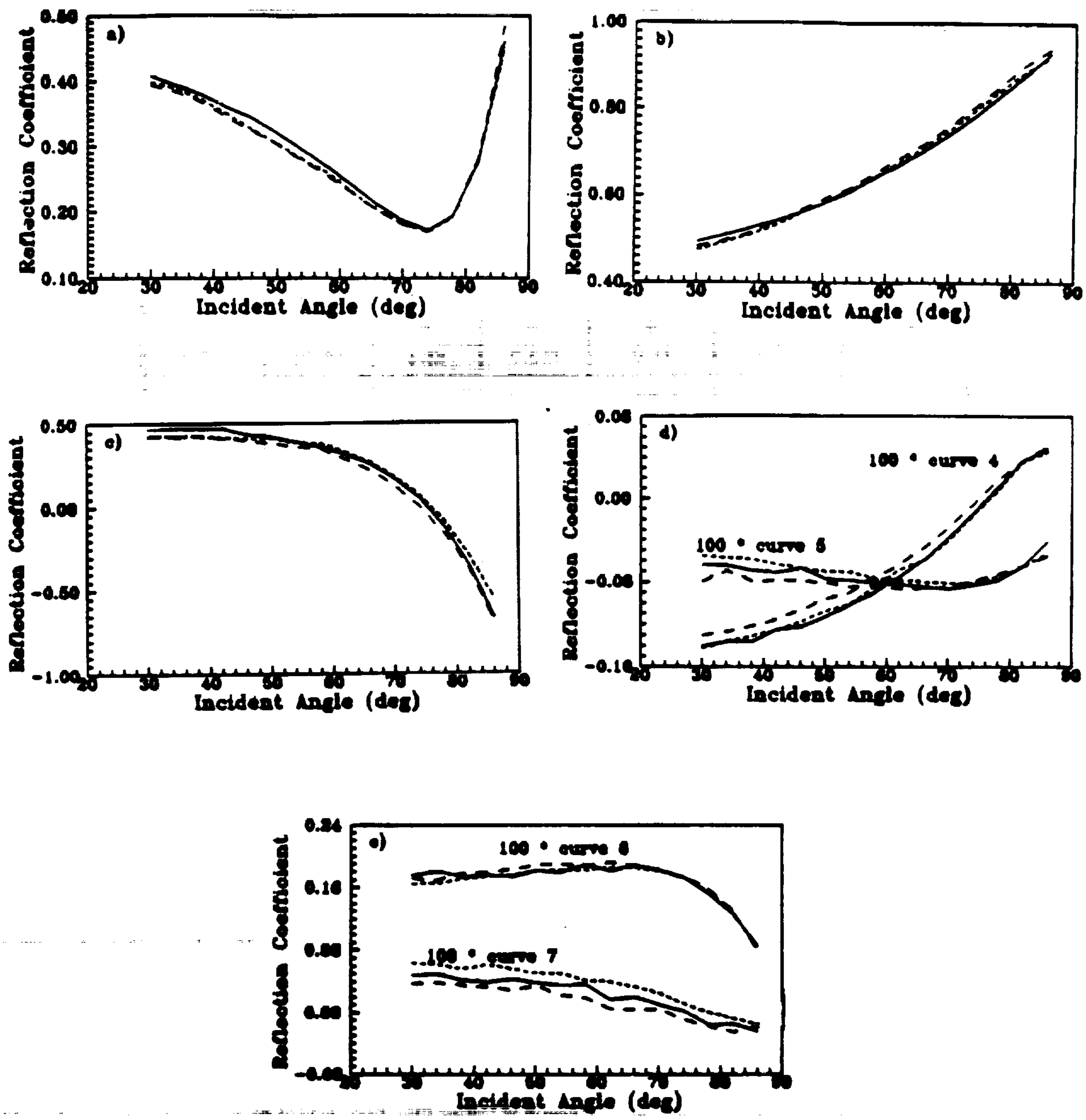

Figure 7. Reflection coefficient measurements for the case that the detector angles are at the calibrated angle ("————" line), 2° off ("- - - -" line) and -2° off ("— — —" line), respectively, for systematic error analysis.

Table VII. Measurements for the case that the detector angle is ±2° off the calibrated angle for the Co/Pd sample.

	average (no shift)	σ_{n-1} (no shift)	detector off 2°	Δ (off 2°)	detector off -2°	Δ (off -2°)
n	1.54	0.2	1.77	0.23	1.33	-0.21
k	3.79	0.07	3.78	-0.01	3.68	-0.11
ε_{xx}	-12.1 + i11.4	0.3 + i1.0	-11.1 + i13.5	1.0 + i2.1	-11.77 + i9.44	0.33 + -i2.0
ε_{xy}	0.145 — i0.107	0.006 — i0.013	0.135 — i0.149	-0.010 — i0.042	0.140 — i0.086	-0.005 — -i0.021
Q	1.3	—	1.2	—	1.6	—
DME (%)	3.0	—	2.9	—	4.0	—
θ_k	0.203	0.002	0.201	-0.002	0.215	0.012
ϵ_k	0.075	0.004	0.084	0.009	0.079	0.004
R	0.446	0.008	0.443	-0.003	0.432	-0.014

To study the possible effect of the three remaining systematic error sources, we measured the dielectric tensor with the polarizer, quarterwave plate and detector module deviated ±2° off the given angle, respectively, for the same Co/Pd sample which was used for the random error analysis. Figure 5 shows the measured reflection curves for the polarizer at normal position, off +2° and off -2° positions. The same measurements for the quarterwave plate and detector module are shown in Figs. 6 and 7, respectively. The calculated variation on the dielectric tensor, Kerr rotation, ellipticity and reflectivity for these systematic angle changes are listed in Table V, VI, and VII.

The variation on the measured results for the polarizer ±2° off is small and even within the random error range. Since the accuracy of the polarizer angle is better than that, it will cause no systematic error problem. The variation on the measured results for the quarterwave plate ±2° off is much larger and more attention needs to be paid for the accuracy of this angle. The resolution of this angle is about 0.25° and an accuracy of less than 1° can be achieved. This could make the possible systematic error much smaller. The variation on the results for the detector box angle ±2° off is between the above two cases. The accuracy of this angle is about 1° and the systematic error should therefore be under control.

Another way to check the systematic error is to compare the measured Kerr rotation angle, ellipticity and reflectivity with other established characterization system, like the MOKS system. The good agreement on the Kerr rotation, ellipticity and reflectivity measurements between these two systems (see Tables III and IV) also indicates that the systematic error in this VAMOE system is insignificant.

III. DIELECTRIC TENSOR FOR TbFe AND Co/Pt SAMPLES

Dielectric tensor characterization for the M-O samples is important for both understanding and application of these materials. Thickness dependence of the dielectric tensor for Co/Pd superlattice multilayered film has been studied in our previous paper,[16] and we found that both diagonal and off-diagonal elements of the tensor are more or less constant for film thicknesses greater than 150 Å. In the same paper, we also have studied the composition dependence of the dielectric tensor for both Co/Pt and Co/Pd multilayered films. The enhancement of the off-diagonal element for the multilayered samples over diluted pure cobalt explains the larger M-O Kerr effect for these multilayered samples. In this section, we first present the dielectric tensor measurement for several TbFe and TbFeCo samples with different compositions. Then, more measurements for Co/Pt samples are presented, which extends both the thickness and composition range of the samples for study.

For these TbFe and TbFeCo samples, they all have overcoating, and are with glass substrate. Their hysteresis loops are square. The detailed structural and magnetic data for all the TbFe and TbFeCo samples are listed in Table VIII. Figure 8 shows a typical measurement of the seven reflection curves along with the calculated curves from the matched dielectric tensor values, for sample TB6. The matching between the experimental and calculated reflectivity curves is excellent. All of the data matching errors are less than 6%, as listed in Table VIII. The DME decreases with larger reflectivity value which has better signal-to-noise ratio. The slightly larger difference on the Kerr rotation, ellipticity and reflectivity between the VAMOE and MOKS systems for TbFe and TbFeCo samples than that of the superlattice samples is caused by the higher complexity of the former types of sample. One notices that as TbFe sample changes from the Tb-rich (sample TF6) to Fe-rich (the rest), the off-diagonal element changes sign as well as the Kerr rotation.

Table VIIII lists all the structural and magnetic data for the Co/Pt samples studied here. There is no overcoating for any of them and their hysteresis loops are all square. (They are deposited on glass substrate.) Figure 9 shows a typical measurement for sample COPT3. The typical data for a Co/Pd sample has been shown in the previous error analysis section.

IV. OPTICAL MEASUREMENTS FOR NON-MAGNETIC SAMPLES

The VAMOE system developed for M-O media can also be used to measure the optical properties for various non-magnetic films. Since M-O data storage application also involves the characterizations for the substrate, overcoating and reflecting layer materials, it is useful that this system is able to perform this characterization. In this section, we present the optical refractive index n, absorption coefficient k and film thickness measurements for some non-magnetic materials.

Figures 10 to 13 show the measured reflection coefficient curves as a function of the incident angle for a glass substrate, a dielectric thin film, a sol-gel thin film and an organic polymer film. Table X lists the measurement results for these and other samples. The dielectric and organic polymer films are coated on glass substrate and the sol-gel films are coated on a GaAs substrate with n = 3.85 and k = 0.077.

Series of metallic films of Al, Al-Ti, Cu_3Al, Al_2Cr, Cu and Pt with different thicknesses are measured and their results are listed on Table XI. The typical reflection coefficient curves for each kind are shown in Figs. 14 to 19. The matching between the experimentally measured curves and those computer calculated from the estimated optical constants is quite good. All the DME are less than 3%. Also in this table, we cited the n, k values for Al, Cu and Pt from handbook.[17]

V. SUMMARY

In summary, we have constructed a new and comprehensive dielectric tensor characterization system, both for magneto-optical and non-magnetic thin films, at λ = 632.8 nm. The random and systematic error analysis of

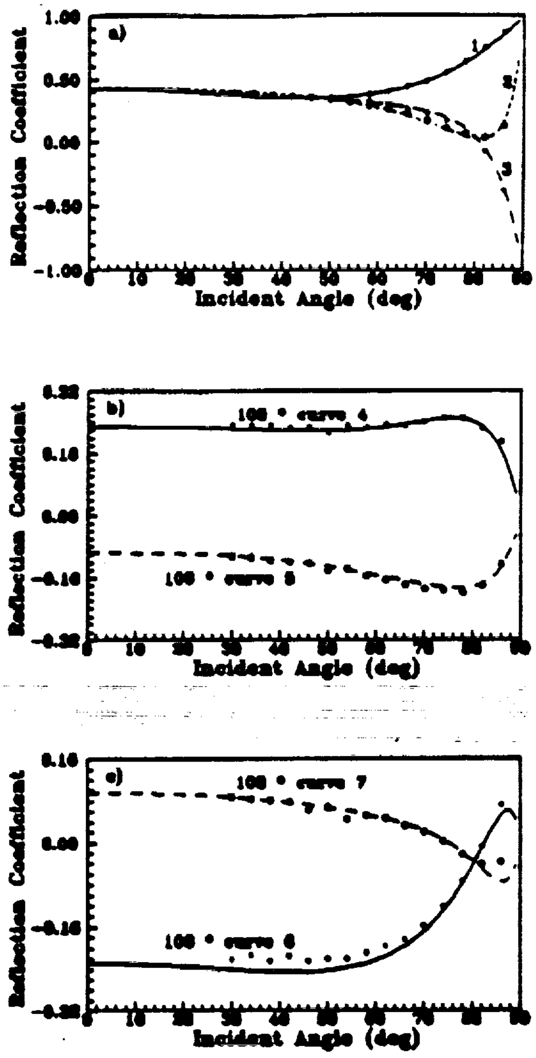

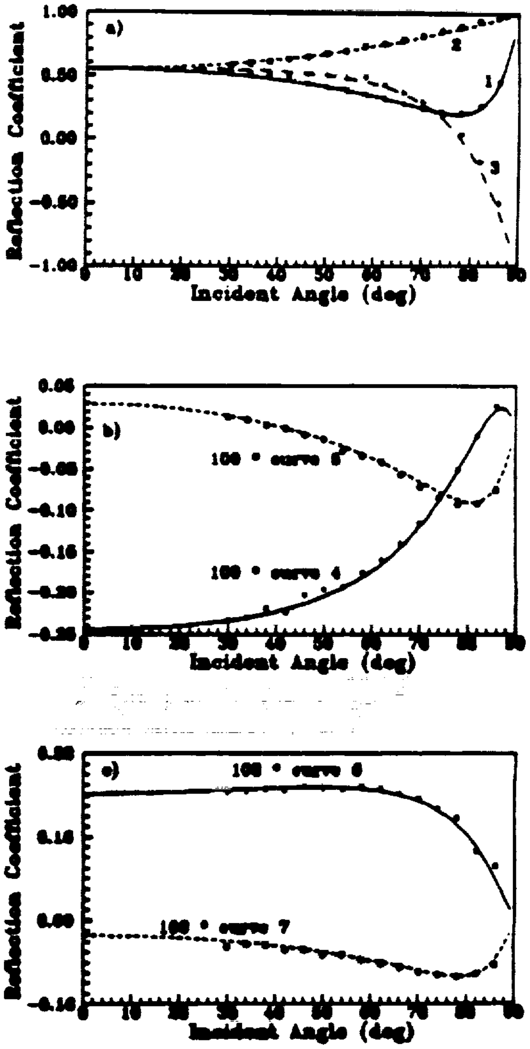

Figure 8. Seven reflection coefficients as function of the angle of incidence for TF6 sample. The symbols (star, circle and cross) are the measured ones and the continuous curves are calculated with the estimated dielectric tensor.

Figure 9. Seven reflection coefficients as function of the angle of incidence for COPT3 sample. The symbols (star, circle and cross) are the measured ones and the continuous curves are calculated with the estimated dielectric tensor.

Table VIII. Measurement results of the TbFeCo and TbFe samples with various film compositions at λ=633nm. The values in the parentheses are measured by the magneto-optic Kerr spectrometer (MOKS) system.

Samples	TF1	TF2	TF3	TF4	TF5	TF6	TF7
MO composition (at. %)	Tb:16.1 Fe:77.0 Co: 6.9	Tb:20.1 Fe:71.3 Co: 8.6	Tb:20.3 Fe:70.9 Co: 8.9	Tb:16.7 Fe:83.3	Tb:14.5 Fe:85.6	Tb:28.1 Fe:71.9	Tb:18.3 Fe:74.5 Ar: 3.6
overcoating thickness (Å)	SiN 647	SiN 800	SiN 800	SiN 757	SiN 791	SiO 1326	SiO 1615
MO film thickness (Å)	431	1000	500	733	726	1354	554
underlayer thickness (Å)	-	-	-	SiN 716	SiN 723	-	-
coercivity (kOe)	2.42	3	2.22	2.24	0.92	1.63	1.26
n	2.32	2.43	2.91	2.30	2.42	2.37	2.72
k	3.78	3.24	3.31	3.23	3.19	3.11	2.85
ε_{xx}	-8.90 + i17.54	-4.60 + i15.80	-2.49 + i18.52	-5.14 + i14.83	-4.22 + i14.67	-3.92 + i15.60	-3.74 + i8.68
ε_{xy}	0.665 + i0.160	0.319 + i0.118	0.417 - i0.033	0.294 + i0.105	0.273 + i0.074	-0.250 - i0.066	0.121 + i0.041
DME (%)	5.4	3.2	3.1	3.0	3.5	3.0	1.2
θ_k(°)	0.675 (0.617)	0.631 (0.591)	0.679 (0.660)	0.738 (0.699)	0.682 (0.642)	-0.311 (-0.310)	0.189 (0.193)
ϵ_k(°)	-0.245 (-0.319)	0.033 (0.047)	0.077 (0.081)	0.044 (0.039)	0.034 (0.036)	0.129 (0.120)	-0.088 (-0.077)
R	0.180 (0.186)	0.301 (0.316)	0.221 (0.229)	0.246 (0.250)	0.240 (0.242)	0.419 (0.416)	0.501 (0.457)

Table VIIII. Measurement results of the Co/Pt samples with various film compositions at $\lambda=633nm$. The values in the parentheses are measured by the magneto-optic spectrometer (MOKS) system.

sample	COPT1	COPT2	COPT3	COPT4
composition of Co/Pt in Å	2.4/9.6	7.2/23.8	2.4/7.2	3/10
Co content	0.20	0.23	0.25	0.23
number of bilayers	14	12	17	20
MO film thickness (Å)	180	180	180	260
coercivity (kOe)	0.62	0.70	0.44	2.24
n	1.71	1.99	2.19	2.18
k	4.67	4.67	4.45	4.13
ε_{xx}	-18.9 + i16.0	-17.9 + i15.8	-15.3 + i17.6	-13.2 + i14.8
ε_{xy}	0.251 - i0.040	0.390 - i0.040	0.365 - i0.070	0.165 - i0.008
DME (%)	4.9	4.3	3.4	2.8
θ_k(°)	0.165 (0.16)	0.243 (0.23)	0.255 (0.24)	0.119 (0.114)
ε_k(°)	0.017 (0.01)	-0.018 (-0.02)	-0.030 (-0.03)	-0.013 (-0.012)
R	0.59 (0.60)	0.58 (0.57)	0.55 (0.53)	0.604 (0.612)

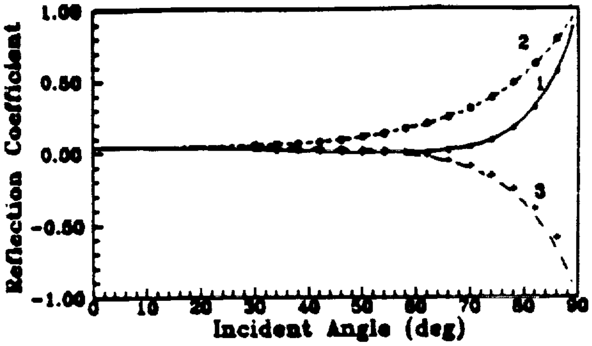

Figure 10. Three reflection coefficients as function of the angle of incidence for the glass sample on Table X. The symbols (star, circle and cross) are the measured ones and the continuous curves are calculated with the estimated n = 1.500, and k = 0 from the multilayer analysis program.

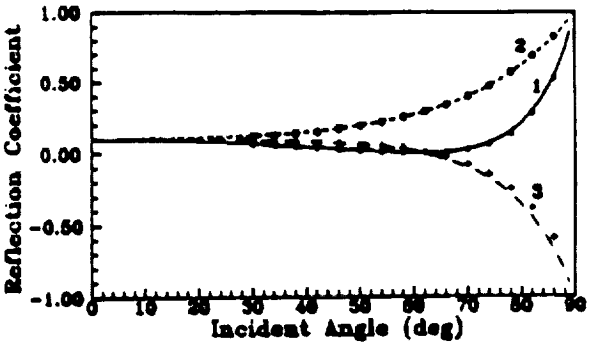

Figure 11. Three reflection coefficients as function of the angle of incidence for the dielectric film listed on Table X. The symbols (star, circle and cross) are the measured ones and the continuous curves are calculated with the estimated n = 2.12, k = 0 and film thickness = 235 Å from the multilayer analysis program.

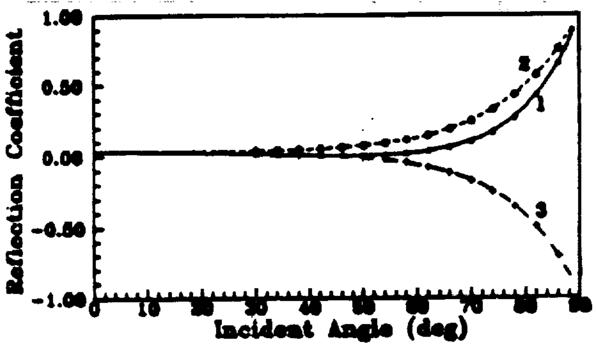

Figure 12. Three reflection coefficients as function of the angle of incidence for the sol-gel (high index) film listed on Table X. The symbols (star, circle and cross) are the measured ones and the continuous curves are calculated with the estimated n = 2.17, k = 0 and film thickness = 83 Å from the multilayer analysis program.

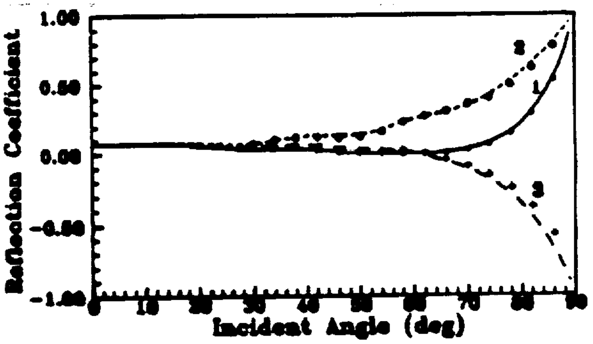

Figure 13. Three reflection coefficients as function of the angle of incidence for the organic polymer sample 9-D, listed on Table X. The symbols (star, circle and cross) are the measured ones and the continuous curves are calculated with the estimated n = 1.68, k = 0.030 and film thickness = 2700 Å from the multilayer analysis program.

Table X. Measurement results of several non-magnetic and non-metal materials at $\lambda = 633\text{nm}$.

sample	n	k	film thickness (Å)	under-layer (Å)	DME (%)
Corning micro slide #2941	1.500	0	10^7	0	2.3
ZrO_2 dielectric	2.120	0	235	0	2.3
Sol-gel (high index)	2.17	0	83	0	0.8
Sol-gel (low index)	1.45	0	84	0	1.1
Organic polymer 7-D	1.71	0.010	5300	265 (ITO)	6.0
Organic polymer 9-B	1.61	0.044	1500	265 (ITO)	4.7
Organic polymer 9-D	1.68	0.030	2700	265 (ITO)	4.7

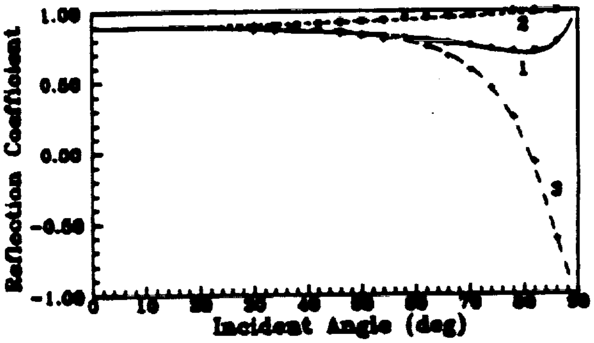

Figure 14. Three reflection coefficients as function of the angle of incidence for the aluminum sample #3, listed on Table XI. The symbols (star, circle and cross) are the measured ones and the continuous curves are calculated with the estimated $n = 1.05$, $k = 5.88$ and film thickness = 800 Å from the multilayer analysis program.

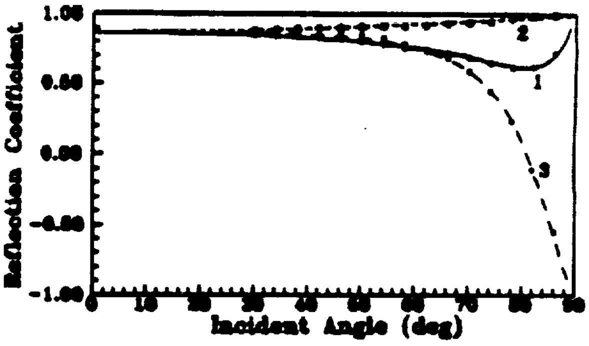

Figure 15. Three reflection coefficients as function of the angle of incidence for the Al-Ti sample #2, listed on Table XI. The symbols (star, circle and cross) are the measured ones and the continuous curves are calculated with the estimated $n = 1.45$, $k = 6.11$ and film thickness = 1000 Å from the multilayer analysis program.

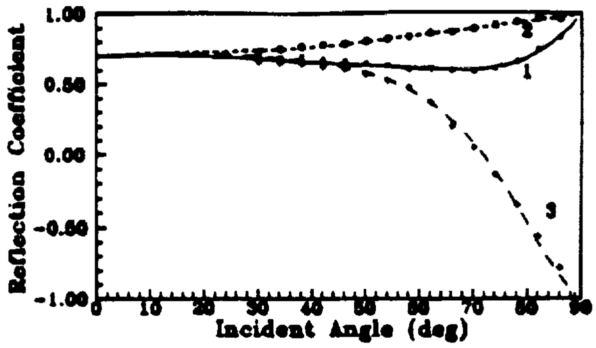

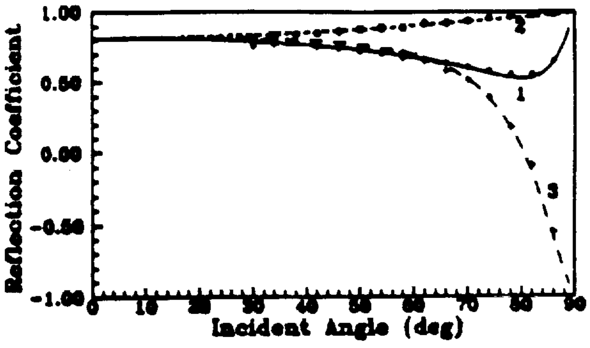

Figure 16. Three reflection coefficients as function of the angle of incidence for the Cu$_3$Al sample #1, listed on Table XI. The symbols (star, circle and cross) are the measured ones and the continuous curves are calculated with the estimated n = 1.41, k = 4.53 and film thickness = 500 Å from the multilayer analysis program.

Figure 17. Three reflection coefficients as function of the angle of incidence for the Al$_2$Cr sample #2, listed on Table XI. The symbols (star, circle and cross) are the measured ones and the continuous curves are calculated with the estimated n = 1.76, k = 5.53 and film thickness = 800 Å from the multilayer analysis program.

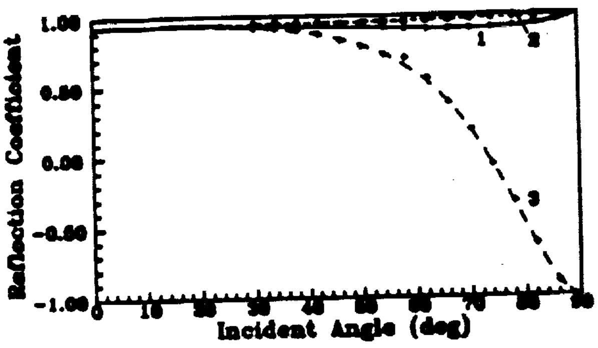

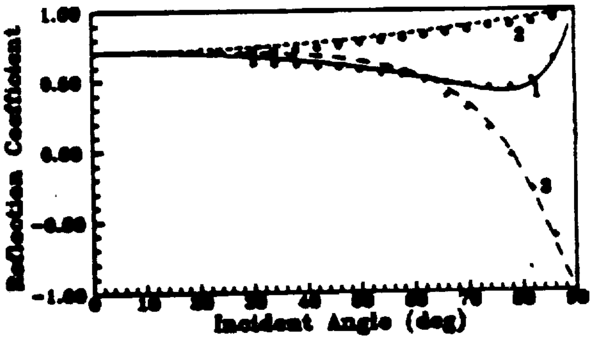

Figure 18. Three reflection coefficients as function of the angle of incidence for the copper sample #2, listed on Table XI. The symbols (star, circle and cross) are the measured ones and the continuous curves are calculated with the estimated n = 0.41, k = 5.83 and film thickness = 1000 Å from the multilayer analysis program.

Figure 19. Three reflection coefficients as function of the angle of incidence for the platinum film, listed on Table XI. The symbols (star, circle and cross) are the measured ones and the continuous curves are calculated with the estimated n = 1.72, k = 4.05 and film thickness = 1510 Å from the multilayer analysis program.

Table XI. Measurement results of several non-magnetic metal samples with various film thicknesses at λ=633nm.

sample	over-coating (Å)	n	k	film thickness (Å)	DME (%)
Al #1	0	1.01	6.25	223	2.7
Al #2	0	1.05	5.83	500	2.3
Al #3	0	1.05	5.88	800	1.5
Al #4	0	1.03	5.97	1000	2.1
Al-Ti #1	0	1.67	6.08	438	1.9
Al-Ti #2	0	1.45	6.11	1000	1.1
Al-Ti #3	0	1.60	6.32	488	2.1
Al-Ti #4	0	1.35	5.51	650	1.5
Cu_9Al #1	166 (ZrO_2)	1.41	4.53	500	1.9
Cu_9Al #2	138 (ZrO_2)	1.31	4.59	1000	1.8
Al_2Cr #1	0	1.76	5.65	500	1.8
Al_2Cr #2	0	1.76	5.53	800	1.9
Cu #1	165 (ZrO_2)	0.48	5.42	500	2.3
Cu #2	173 (ZrO_2)	0.41	5.83	1000	1.3
Pt	0	1.72	4.05	1510	1.4
Al from handbook	–	1.396	7.650	infinite	–
Cu from handbook	–	0.24	3.450	infinite	–
Pt from handbook	–	2.330	4.150	infinite	–

the system was carried out to assure the accuracy and precision of the measurements. The dielectric tensor measurements for TbFe, TbFeCo, Co/Pt and Co/Pd thin films reveal valuable information about their optical and magneto-optical properties, and it helps their application performance improvement. This system also gives an accurate way to characterize the optical properties for non-magnetic multilayered thin films.

VI. REFERENCES

1. R. M. A. Azzam, and N. M. Bashara, *Ellipsometry and Polarized Light*, North-Holland, New York (1977).
2. D. Weller and W. Reim, H. Ebert, D. Jonson, and F. Pinski, "Correlation Between Bandstructure and Magneto-optical Properties of BCC Fe_xCo_{1-x}," Journal De Physique, Colloque C8, Supplement au n° 12, Tome 49, 41-42 (1988).
3. S.-C. Shin, and A. C. Palumbo, "Magneto-optical Properties of Co/Pd Superlattice Thin Films," J. Appl. Phys. 67(1), 317-320 (1990).
4. W. B. Zeper, F. J. A. M. Greidanus, P. F. Carcia, and C. R. Fincher, "Perpendicular Magnetic Anisotropy and Magneto-optical Kerr Effect of Vapor Deposited Co/Pt Layered Structures," J. Appl. Phys. 65(12), 4971-4975 (1989).
5. M. Mansuripur, F. L. Zhou, and J. K. Erwin, "Measuring the wavelength dependence of magnetooptical Kerr (or Faraday) rotation and ellipticity: a technique," Appl. Opt. 29, 1308-1311 (1990).
6. F. L. Zhou, J. K. Erwin and M. Mansuripur, "Spectral measurements of the magneto-optical Kerr rotation and ellipticity in the media of optical recording", J. Appl. Phys. 69(8), 5091-5093 (1991).
7. P. He, W. A. McGahan, J. A. Woollam, F. Sequeda, T. McDaniel, and H. Do, "Magneto-optical Kerr Effect and Perpendicular Magnetic Anisotropy of Evaporated and Sputtered Co/Pt Multilayer Structures," J. Appl. Phys. 69(7), 4021 (1991).
8. P. N. Argyres, "Theory of the Faraday and Kerr Effects in Ferromagnetics," Phys. Rev 97, 334 (1955).
9. G. A. N. Connell, "Measurement of the Magnetooptical Constants of Reactive Metals," Appl. Opt. 22, 3155-3159 (1983).
10. S. Hashimoto, Y. Ochiai, and K. Aso, "Film Thickness Dependence of Magneto-optical and Magnetic Properties in Co/Pt and Co/Pd Multilayers," J. Appl. Phys. 67(9), 4429-4431 (1990).
11. A. C. Palumbo and S.-C. Shin, "Thickness Dependence of Magneto-optical Effects in Ultrathin Multilayered Co/Pd Films," SPIE 1316, 363-366 (1990).
12. M. Ruane, M. Mansuripur, and R. Rosenvold, "Measurement of Reflectivities for Magnetooptical Media," Appl. Opt. 25, 1946-1951 (1986).
13. M. Mansuripur, M. Ruane, and R. Rosenvold, "Apparatus for Measuring Reflectivity", U.S. patent #4,838,695, June (1989).
14. M. Mansuripur, "Analysis of Multilayer Thin-film Structures Containing Magneto-optical and Anisotropic Media at Oblique Incidence Using 2×2 Matrices," J. Appl. Phys. 67, 6466-6475 (1990).
15. L. D. Landau and E. M. Lifshitz, *Statistical Physics*, 379-406, Pergamon, London (1958).
16. A. F. Zhou, J. K. Erwin, C. F. Brucker and M. Mansuripur, "Dielectric Tensor Characterization for Magneto-Optical Recording Media," accepted by Appl. Opt.
17. *Handbook of Chemistry and Physics*, CRC Press, Boca Raton, Florida (1989).

APPENDIX D